Triphenylamine-based conjugated microporous polymers as dye adsorbents and supercapacitors

Mohammed G. Kotp[a], Santosh U. Sharma[b], Jyh-Tsung Lee[b], Ahmed F.M. EL-Mahdy[a,*], Shiao-Wei Kuo[a,c,*]

[a] Department of Materials and Optoelectronic Science, Kaohsiung, 80424, Taiwan
[b] Department of Chemistry, National Sun Yat-Sen University, Kaohsiung 80424, Taiwan
[c] Department of Medicinal and Applied Chemistry, Kaohsiung Medical University, Kaohsiung, 807, Taiwan

ARTICLE INFO

ABSTRACT

Background: Conjugated microporous polymers CMPs have unique position among porous materials thus they are studied widely. Realistically, triphenylamine (TPA) derivatives generally possess high aromaticity, redox capabilities, high charge motilies, and outstanding electronic features, therefore designing CMPs based on TPA derivatives could result in fantastic properties.

Methods: We performed one-pot coupling and polycondensation of a boronated triphenylamine derivative (TPA-3Bor) with bromobenzene (Bz-4Br) and bromopyrene (Py-4Br) derivatives to obtain two new TPA-based conjugated microporous polymers (TPA-Bz and TPA-Py CMPs, respectively). The successful synthesis of two TPA CMPs and their features were examined via Fourier transform infrared (FTIR) and ^{13}C solid state NMR spectroscopies.

Significant Findings: These two CMPs displayed attractive adsorptive properties toward the small dye molecule rhodamine B (RhB) from an aqueous solution. Outstanding adsorption performance, rapid kinetics, and good reusability suggest that our CMPs could function as effective adsorbents for RhB and, perhaps, other pollutants from wastewater. Moreover, our TPA-based CMPs displayed effective and stable performance when introduced as electrodes for supercapacitors, with capacitances as high as 78 F g^{-1} at a current density of 1 A g^{-1} as well as high stability. This study emphasizes the importance of conjugation and planarity in the future design of such materials.

© 2022 Taiwan Institute of Chemical Engineers. Published by Elsevier B.V. All rights reserved.

Introduction

Conjugated microporous polymers (CMPs), first prepared by Andrew Cooper [1], are unique among porous materials because of their π-conjugated frameworks, three-dimensional (3D) lattices, and permanently microporous structures [2−9]. Despite similarities in the syntheses through coupling of porous aromatic frameworks and CMPs, the former possess tetrahedral tetraphenylmethane nodes and, therefore, do not feature extended π-conjugated systems [10−13]. To some extent, covalent triazine frameworks contain the same microporous features as those in CMPs, but they are prepared using different chemistry [2, 14]. CMPs can be created from two or more monomers or through homocoupling of singular monomers [15−18]; the customization of CMPs is almost boundless, with great scope for tuning their pore structures, morphologies, and optoelectronic behavior through tuning of the topologies of their monomers

or through doping with various heteroatoms or metals [5, 19-21]. Many reactive coupling partners (e.g., halogens, boronic acids, alkenes, alkynes, amines, nitriles, and substituted aromatic monomers) [22−27] have been applied in the synthesis of CMPs.

The most prevalent routes toward CMPs have involved Sonogashira−Hagihara coupling, Suzuki−Miyaura coupling, Heck coupling, Yamamoto coupling, phenazine ring fusion, cyclotrimerization, and Schiff-base condensation [28−32]. Various features have been elucidated to favor CMPs having extended conjugated structures, high porosities, tunable chemistry, and outstanding thermal and chemical robustness [33−37]. Nevertheless, the quest remains to develop new CMPs possessing unique porosities, elegant geometries, and higher thermal resistance. With their attractive features, CMPs have found many applications in, for example, storing and separating gasses, chemical encapsulation, photocatalysis, heterogeneous catalysis, light emitting diodes, sensors, and energy storage and conversion [38, 39].

Water scarcity crisis is a global challenge thus increasing the availability of potable water through water purification techniques could contribute well to solve this problem, thus new materials have been designed for water purification [40−48]. Organic dyes are

* Corresponding author.
E-mail addresses: ahmedelmahdy@mail.nsysu.edu.tw (A.F.M. EL-Mahdy), kuosw@faculty.nsysu.edu.tw (S.-W. Kuo).

common organic water contaminants arising from industrial, pharmaceutical, and biological activities [49, 50]. Because they can have harmful effects on the health of living organisms [51], ecosystems [49], and the general public, the majority of commercial dyestuffs are categorized as very toxic agents, deleterious to aval organisms, carcinogenic, and non-biodegradable, making their removal from wastewater a high priority. Although various strategies (e.g., ion exchange and photocatalysis) have been introduced to eliminate such hazardous materials [52–55], their adsorption from wastewater is most common because of cost-effectiveness and eco-friendliness [56]. Various families of porous materials—including natural fibers, ordered mesoporous carbons (OMCs), zeolites, and metal organic frameworks (MOFs) [46, 57-59] have been examined as dye adsorbents. Relatively poor removal performance, adsorption efficacy, and recyclability have minimized the efficacy of zeolites and natural fibers as dye adsorbents [60]. Furthermore, MOFs generally possess low stabilities, due to their weak coordinative metal−organic bonds, and OMCs have the drawback of requiring high-temperature thermal treatment during their synthesis [61, 62]. Consequently, there remains a challenge to develop new adsorbents capable of the efficient adsorption and disposal of dyestuffs with rapid kinetics.

Because triphenylamine (TPA) derivatives generally possess high aromaticity, redox capabilities, high charge mobilities, and outstanding electronic features, designing CMPs based on TPA derivatives could result in high adsorptivities [63, 64]. In addition, TPA derivatives have also been applied as electrode substrates for storing energy in various types of supercapacitors, the result of their attractive charge transport features, morphologies, thermal stabilities, and excellent electroluminescence properties [65, 66]. Furthermore, reversible radical redox processes have been observed during charging and discharging processes when applying polymeric TPA moieties [67]. Thus, we suspected that new electrochemically stable and conducting porous polymers, with tunable pore sizes and high surface areas, could be derived from new TPA derivatives to streamline the diffusion rates of solvents and electrolyte molecules.

In this study, we prepared two TPA-based CMPs -TPA-Bz CMP and TPA-Py CMP- in one step through classical Suzuki coupling between tris(4-(4,4,5,5-tetramethyl-1,3,2-dioxaborolan-2-yl)phenyl)amine (TPA-3Bor) with 1,2,4,5-tetrabromobenzene (Bz-4Br) and 1,3,6,8-tetrabromopyrene (Py-4Br), respectively (Scheme 1). Both of TPA CMPs featured high surface areas up to 1470 $m^2 g^{-1}$, relative thermal stabilities with a char yield reached 87% after heating to 800 °C, and chemical resistance. Adsorption efficiencies of TPA CMPs for

the small dye molecule rhodamine B (RhB) from water were recorded (up to 1633 mg g^{-1}) which they are higher than those of other recently reported adsorbents. Moreover, when examined as supercapacitors and displayed a capacitance up to 78 F g^{-1} at current density 1 A g^{-1}. These new TPA CMPs provided efficiencies higher than those of other recently reported TPA derivatives and porous materials.

Experimental section

Materials

Solvents and other chemicals were purchased from commercial sources and applied without further purification. Bromine, pyrene, triphenylamine, and bis(pinacolato)diboron were purchased from Alfa Aesar. Tetrakis(triphenylphosphine)palladium(0) [Pd(PPh₃)₄], *N*-bromosuccinimide (NBS), 1,2,4,5-tetrabromobenzene (Bz-4Br), and potassium carbonate (K₂CO₃) were obtained from Sigma−Aldrich. The syntheses of TPA-3Bor and Py-4Br are presented in Schemes S1−S3. Water was distilled twice prior to use.

TPA-Bz CMP

As presented in Scheme S4, a 30-mL Schlenk tube was charged with TPA-3Bor (200 mg, 0.321 mmol), Bz-4Br (94.8 mg, 0.240 mmol), K₂CO₃ (333 mg, 2.40 mmol), and Pd(PPh₃)₄ (50.0 mg, 0.0430 mmol) and then evacuated for 15 min. *N,N*-Dimethylformamide (DMF, 10 mL) and water (1.34 mL) were added as co-solvents. The tube was subjected to three freeze/thaw cycles (10 min per each cycle), then closed and heated at 130 °C with magnetic stirring for 72 h. The solid was filtered off and washed (three times each) with water, MeOH, and tetrahydrofuran (THF). The gray powder was dried at 100 °C for 24 h.
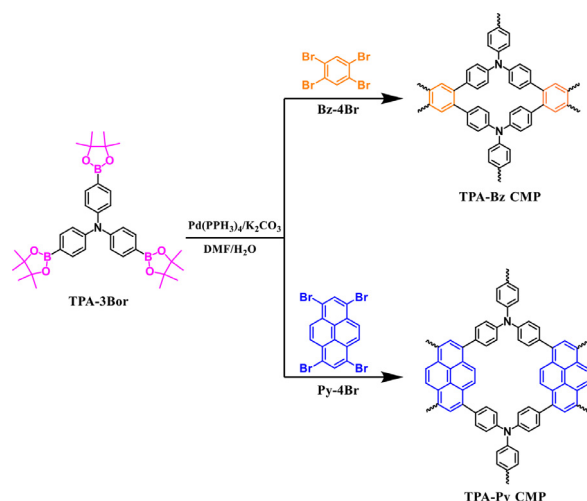
TPA-Py CMP

As presented in Scheme S5, the reaction of TPA-3Bor (200 mg, 0.321 mmol), Py-4Br (125 mg, 0.241 mmol), K₂CO₃ (333 mg, 2.40 mmol), and Pd(PPh₃)₄ (50.0 mg, 0.0430 mmol) in DMF (10 mL) and water (1.34 mL) was performed, using the procedure described above, to give a green powder.

Results and discussion

Materials characterization

For this study, we selected three building blocks for their distinct features: TPA, -a non-basic molecule relative to other amines- and its derivatives, for its promising electrical conductivity [63]; pyrene (Py) for its polycyclic aromatic structure and strong π-stacking ability; and benzene (Bz) for its aromaticity, but lower degrees of conjugation and planarity with respect to Py. We prepared TPA-Bz CMP and TPA-Py CMP through Suzuki coupling of TPA-3Bor with Bz-4Br and Py-4Br, respectively, in the presence of a Pd catalyst; their syntheses are summarized in Scheme 1 and detailed in Schemes S4 and S5. Fourier transform infrared (FTIR) and nuclear magnetic resonance (NMR) spectroscopy confirmed the chemical structures of the synthesized building blocks. We synthesized TPA-3Br as displayed in Scheme S1; its FTIR spectrum featured characteristic absorption signals at 3064, 1570, 1266, and 816 cm^{-1} representing the stretching vibrations of aromatic C−H, C−N, C = C, and C−Br bonds, respectively (Fig. S1). The ^{1}H NMR spectrum of TPA-3Br (Fig. S4) confirmed its aromatic structure through the appearance of two singlets at 7.35 and 6.92 ppm; furthermore, the signals of the nuclei of its aromatic carbon atoms appeared in the ^{13}C NMR spectrum (Fig. S5) as four bands in the range 146−116 ppm. TPA-3Br underwent boronation to yield TPA-3Bor

Scheme 1. Synthesis and 3D structures of the two new CMPs based on TPA units (Reaction proceeded in DMF media, at 130 °C and under N₂ pressure).

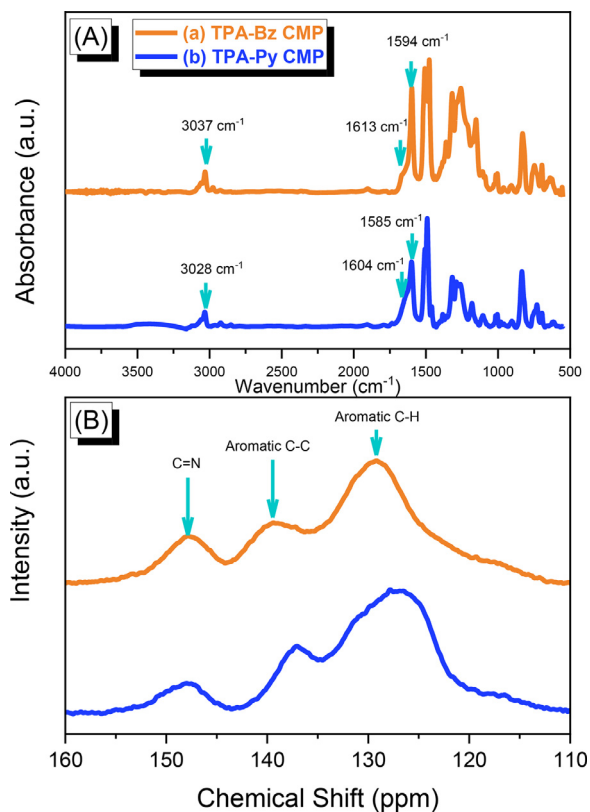**Fig. 1.** (A) FTIR and (B) solid state ^{13}C NMR spectra of (a) TPA-Bz and (b) TPA-Py CMPs.

Fig. 2. Thermogravimetric analysis (a) TPA-Bz and (b) TPA-Py CMPs under a nitrogen media and a heating rate of 20 °C min^{-1}.

(Scheme S2). FTIR spectroscopy revealed the absorption bands for its B−O and C−O bonds at 1517 and 1400 cm^{-1}, respectively (Fig. S1). ^{1}H NMR spectral analysis (Fig. S6) revealed a singlet at 1.34 ppm and two doublets at 7.68 and 7.05 ppm, related to aliphatic and aromatic protons, respectively. The ^{13}C NMR spectrum featured signals for aliphatic and aromatic carbon nuclei at 24.94 and 150−84 ppm, respectively (Fig. S7). The FTIR spectrum of Py-4Br featured characteristic bands for the aromatic C−H, C = C, and C−Br bonds at 3078, 1587, and 862 cm^{-1}, respectively; its low solubility precluded the recording of NMR spectra.

We used FTIR and solid state ^{13}C NMR spectra to elucidate the molecular frameworks of the TPA-Bz and TPA-Py CMPs Fig. 1.a presents the FTIR spectra of our synthesized CMPs. The spectrum of TPA-Bz CMP confirmed the presence of aromatic C−H, C−N, and C = C bonds through the appearance of vibrational bands at 3037, 1613, and 1594 cm^{-1}, respectively. The same vibrational bonds appeared in the spectrum of TPA-Py CMP at 3028, 1604, and 1585 cm^{-1}, with these small shifts arising from differences in their degrees of conjugation. The absence of vibrational bands for B−O and C−B bonds in Figs. S2 and S3 confirmed the complete condensation of the monomers and, thus, the successful syntheses of these CMPs. The solid state ^{13}C NMR spectra (Fig. 1b) revealed evidence for imino carbon nuclei (C−N) and aromatic nuclei. The spectrum of TPA-Bz CMP featured a C−N signal at 147.0 ppm and signals for aromatic carbon nuclei at 139.3 and 129.2 ppm. Similarly, the spectrum of TPA-Py CMP featured these signals at 147.9, 137.1, and 126.9 ppm.
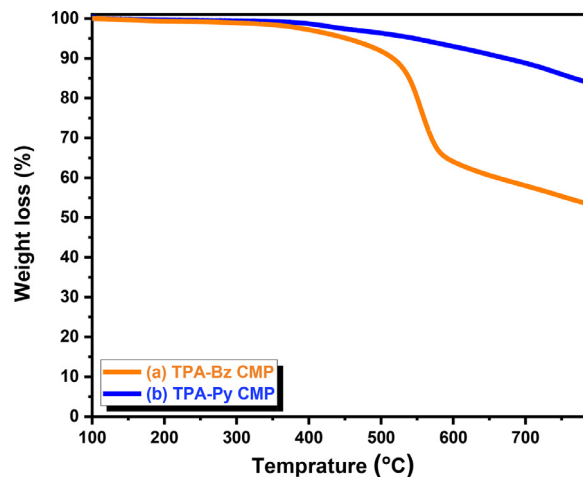
Thermal gravimetric analysis (TGA) confirmed the high degrees of polycondensation of our synthesized TPA-Bz and TPA-Py CMPs and clarified their high thermal robustness. Briefly, Fig. 2 and Table 1 reveal that our CMPs were thermally stable at elevated temperatures under a N$_2$ atmosphere. The thermal resistance of TPA-Py CMP was higher than that of TPA-Bz CMP. The decomposition temperature (T_{d10}) of TPA-Py CMP was 673 °C, with a char yield after heating at 800 °C of 83.7%; for TPA-Bz CMP, these values were 513 °C and 53.1%, respectively. This chasm in the thermal stabilities of these CMPs resulted from the higher degrees of planarity and rigidity of the subunits in the TPA-Py CMP, relative to those in the TPA-Bz CMP, thereby enhancing the strength of π-stacking in the former [15].

We analyzed the porosities of our TPA-Bz and TPA-Py CMPs in terms of their isothermal N$_2$ sorption analytics at 77 K. For both as-synthesized CMPs, Fig. 3 reveals sharp N$_2$ loadings at lower pressure, characteristic of type I isotherms, indicative of microporous frameworks. Using the Brunauer−Emmett−Teller (BET) model, we estimated the surface areas and pore volumes of the as-synthesized CMPs (Table 1). The surface area of TPA-Py CMP (1470 m^2 g^{-1}; Fig. 3b) was higher than that of TPA-Bz CMP (773 m^2 g^{-1}, Fig. 3a), consistent with the higher planarity and flatter structure of the Py units, relative to the Bz units [68]. The TPA-Bz and TPA-Py CMPs possessed pore volumes of 0.681 and 2.11 cm^{-3} g^{-1}, respectively. Furthermore, we applied nonlocal density functional theory (NLDFT) to investigate the distributions of the pore sizes within our CMPs; we calculated (Figs. 3c and 3d and Table 1) a dual micropore size for TPA-Bz CMP (1.3, 1.67 nm), but single-porosity features for TPA-Py CMP (1.09 nm).

We employed field-emission scanning (SEM) and transmission (TEM) electron microscopy to visualize the morphologies of the TPA-Bz and TPA-Py CMPs Figs. 4.a and 3b present SEM images of the TPA-Bz and TPA-Py CMPs, revealing that both possessed spherical shapes without any aggregation. TEM images revealed spherical and smooth structures for both as-synthesized TPA-Bz and TPA-Py CMPs (Figs. 4c and 3d), as well as their loosely aggregated morphologies. Statistical analysis of the TEM data revealed that the average diameter of the particles of TPA-Bz CMP was approximately 83 nm, while that for the

Table 1
Porosity properties and thermal analysis of TPA-Bz, and TPA-Py CMPs.

CMP	Char yield (wt%)	Pore volume (g/cm^3)	Pore size (nm)	Surface area (m^2/g)	$T_{d10\%}$ (°C)
TPA-Bz CMP	53.1	0.68	1.3, 1.67	773	516
TPA-Py CMP	83.7	2.11	1.09	1470	673
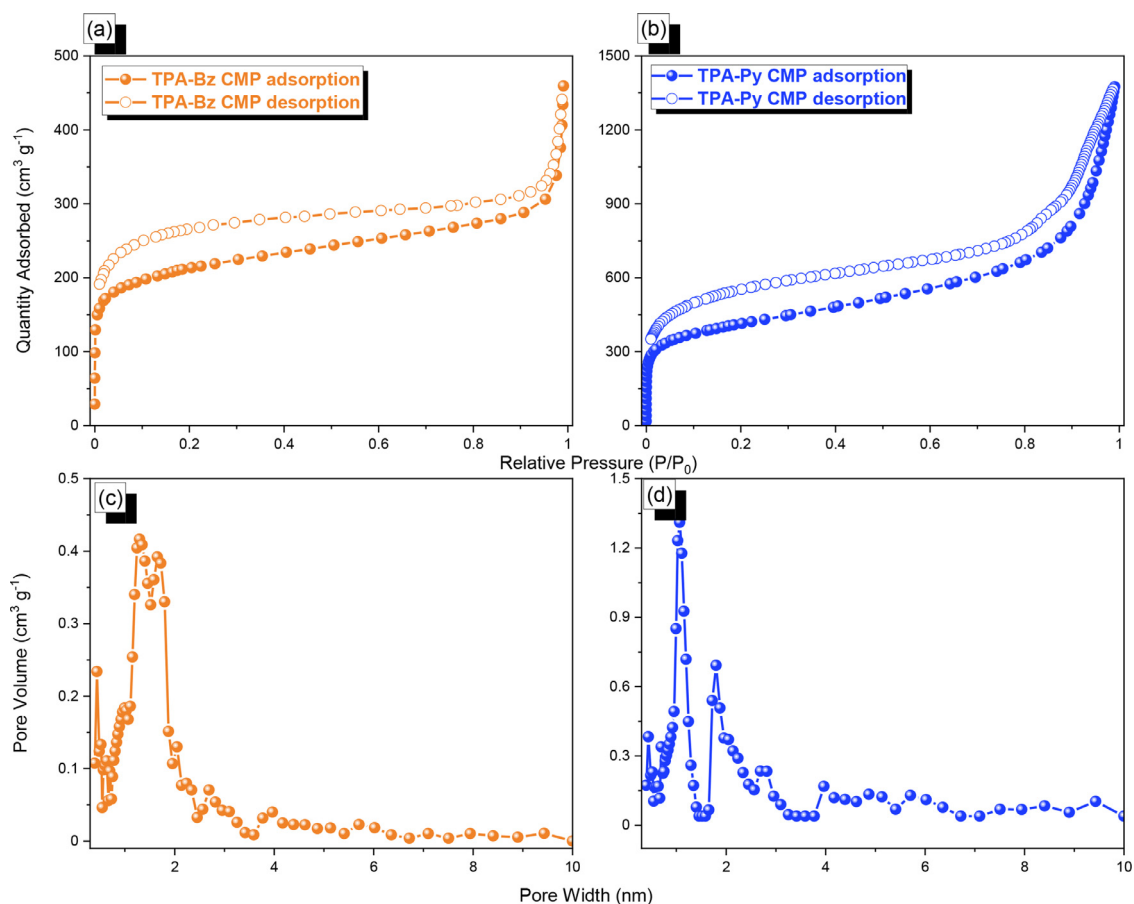
Fig. 3. (a, b) N_2 sorption isotherms and (c, d) pore size distributions of the (a, c) TPA-Bz and (b, d) TPA-Py CMPs at 77 K.

TPA-Py CMP was approximately 16 nm. Thus, TEM confirmed that the planarity of the monomeric building blocks affected the diameter of the resultant CMPs, with the diameter of the more-planar TPA-Py CMP being lower than that of the less-planar TPA-Bz CMP.

Dye removal

RhB is a cationic dyestuff commonly used as a fluorescent tracer for detecting the directions of water flow and their corresponding rates. It is a fluorescent dye that can be detected readily and precisely when using traditional fluorimeters [69, 70]. It is also applied widely as a standard molecule for estimating the features of adsorbents. Because of their high degrees of conjugation, high surface areas, large pore volumes, and hydrophobicity, we suspected that our prepared CMPs would display high efficacy in the adsorption of organic pollutants from water. Accordingly, we evaluated their adsorption behavior in terms of the adsorption of RhB, readily monitored through their UV−Vis profiles at 554 nm. Upon charging 20-mL vials with our prepared TPA-Bz and TPA-Py CMPs (4 mg) and an aqueous solution of RhB (25 mg L^{-1}, 10 mL) and subjecting them to gentle magnetic stirring (400 rpm), the color of the dye disappeared completely within 20 and 5 min, respectively (Figs. 5a and 5b).

Furthermore, the fast loading and efficient adsorption of RhB into our CMPs was also clearly evident in their UV−Vis absorption profiles (Figs. 5c and 5d). The TPA-Bz and TPA-Py CMPs adsorbed up to 74.4 and 99%, respectively, of the RhB within 10 min. We monitored the adsorption of RhB into the TPA-Bz and TPA-Py CMPs though their equilibrium adsorption profiles, then fitted the adsorption data to Langmuir and Freundlich isotherm models [71−74]; Tables S2 and S3 present the respective fitting data. The Langmuir isotherm model

provided correlation coefficients for the TPA-Bz and TPA-Py CMPs of 0.997 and 0.999, respectively (Figs. 6a and 6b); the Freundlich correlation coefficients of TPA-Bz and TPA-Py CMPs (Figs. 6c and 6d) were 0.914 and 0.846, respectively.

The correlation coefficients for the Freundlich model being lower than those for the Langmuir model confirmed that the adsorption of RhB occurred onto our CMPs in the form of monolayers, as well as with homogenous coverage within their pores. Based on the initial concentrations of the supernatant and RhB dyestuff, we calculated the adsorption capacities of the TPA-Bz and TPA-Py CMPs, based on the Langmuir equation (equation S1), from their corresponding calibration curves. The maximum adsorption capacities of the TPA-Bz and TPA-Py CMPs, according to the Langmuir model, toward RhB were 699 and 1633 mg g^{-1}, respectively (Fig. 6a). Thus, the TPA-Py CMP appears to be a much better adsorbent for RhB than the TPA-Bz CMP and all other previously reported CMPs based porphyrin, boron nitride foams, activated carbon, etc. (Table S4). We attribute the much higher adsorption efficacy of RhB onto the TPA-Py CMP, relative to the TPA-Bz CMP, to the higher planarity, greater aromaticity, and larger pores of the former, thereby facilitating physical π-stacking between the CMP and the dyestuff [75]. We suggest that strategies for increasing the degrees of conjugation, aromaticity, and planarity of CMPs should be taken into consideration when developing next-generation dye adsorbents. Furthermore, FTIR spectra of our CMPs after dye adsorption and rinsing featured no additional peaks, confirming that the CMPs and dye molecules interacted physically (Figs. S8a and S8b). Recycling tests of the TPA-Bz and TPA-Py CMPs for the adsorption of RhB revealed only negligible decreases in activity after 10 cycles (Fig. S8c); thus, these CMPs would appear to be excellent adsorbents for purifying wastewater.
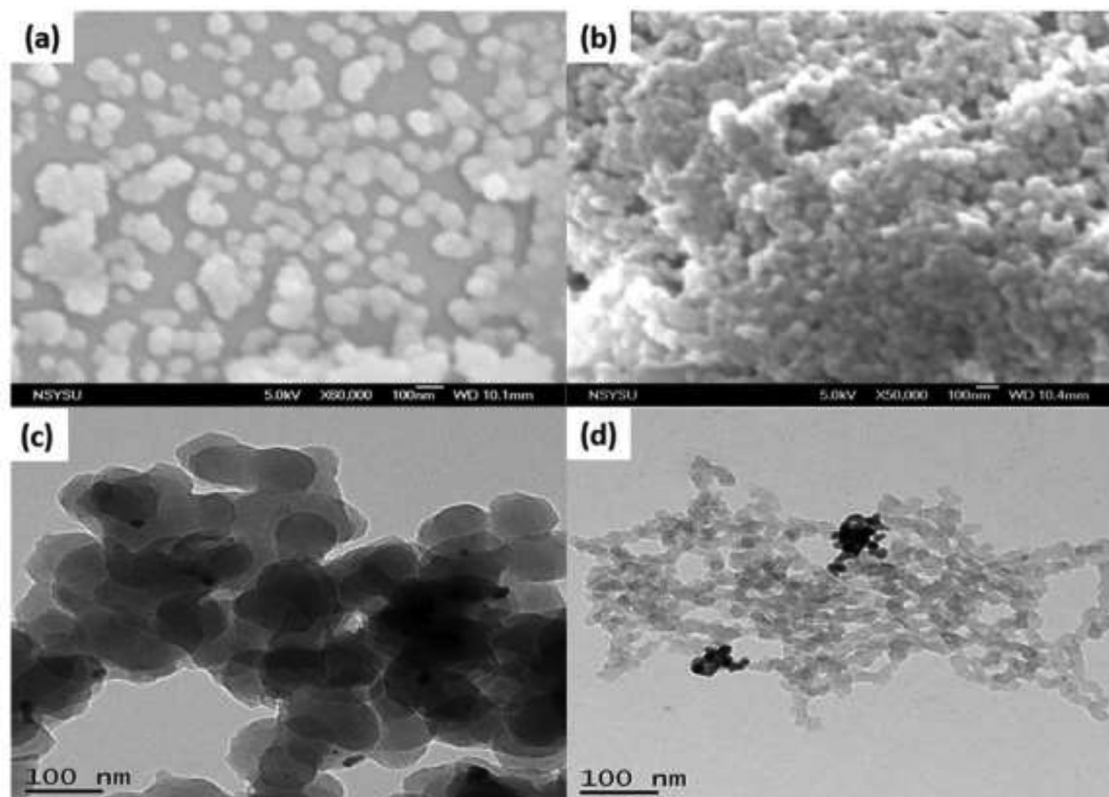
Fig. 4. (a−b) FE-SEM and (c−d) TEM images of the (a, c) TPA-Bz, (b, d) TPA-Py CMPs.
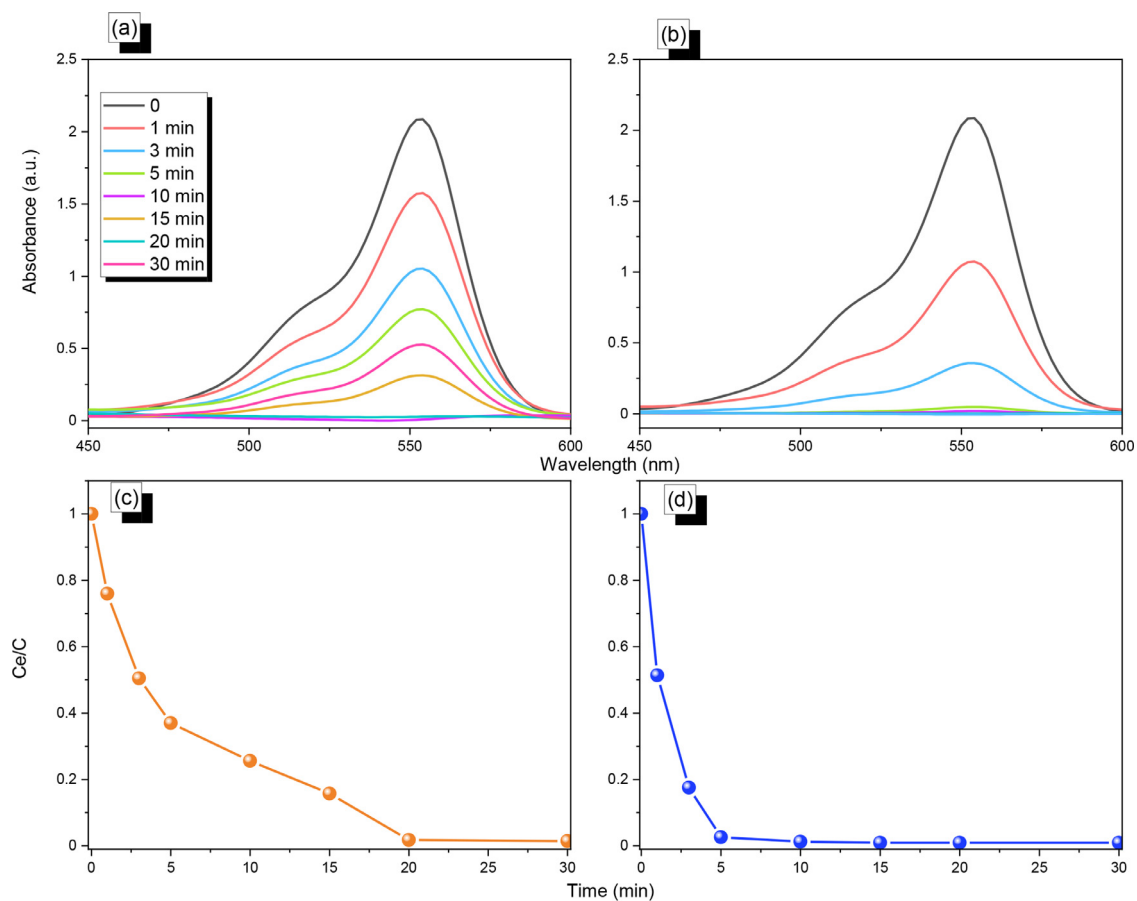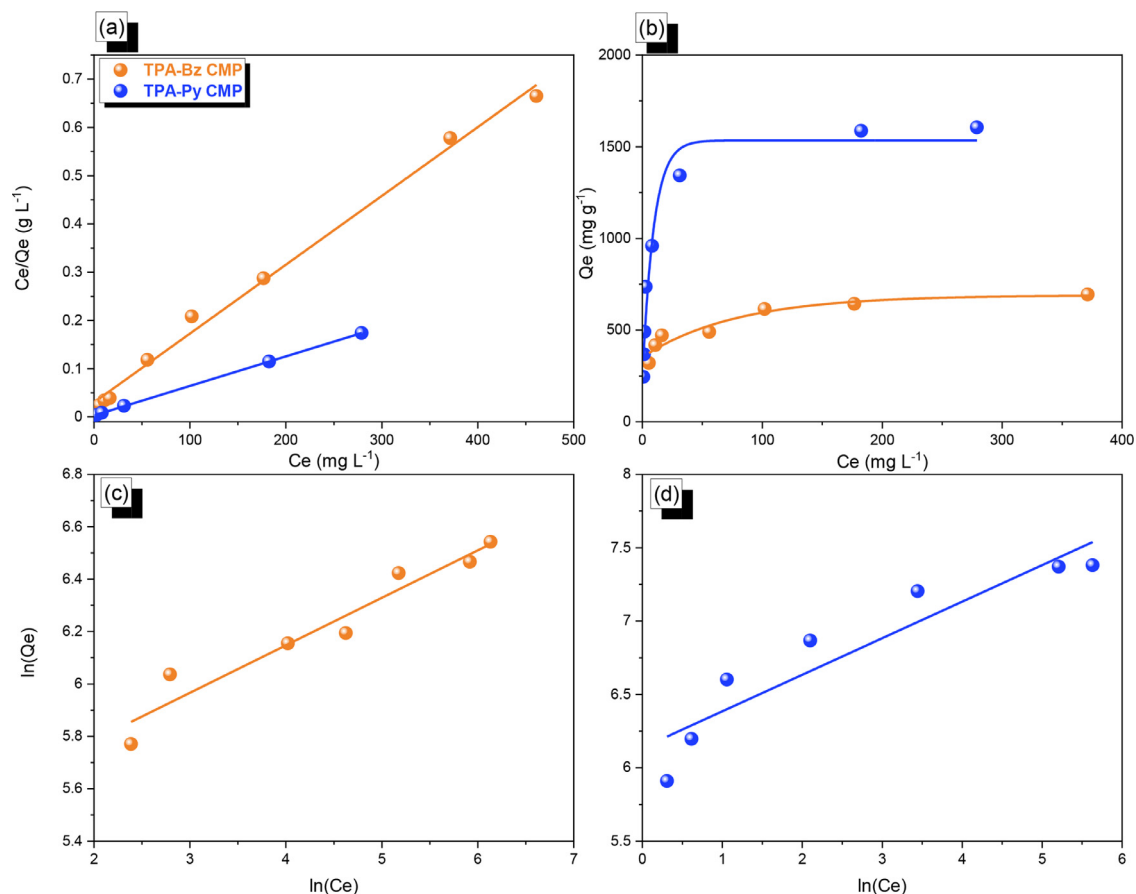

Fig. 5. (a, b) UV−Vis spectra of an aqueous RhB solution (initial concentration: 25 mg L^{-1}) recorded at various time intervals after the addition of the (a) TPA-Bz and (b) TPA-Py CMPs. (c, d) Rates of adsorption of RhB from aqueous solutions (initial concentration: 25 mg L^{-1}) onto the (c) TPA-Bz, and TPA-Py CMPs, measured at various times.

Fig. 6. (a) Langmuir isotherms of TPA-Bz and TPA-Py CMPs. (b) Adsorption isotherms of RhB onto the TPA-Bz and TPA-Py CMPs. (c, d) Freundlich isotherms of RhB onto the (c) TPA-Bz and (d) TPA-Py CMPs.

Electrochemical measurements

In recent times, CMPs have proved to be highly efficient supercapacitor electrodes, arising from the presence of redox-active blocks in their skeletons and the wide variety of potential building blocks. High surface areas, uniform pore sizes, various morphologies, and specificity have resulted in CMPs being efficient materials for storing energy. In this study, we prepared electrodes incorporating our fabricated TPA-Bz and TPA-Py CMPs and estimated their efficiencies in terms of cyclic voltammetry (CV) profiles and galvanostatic charge/discharge (GCD) measurements. We recorded the CV profiles at various scan rates in the range from 5 to 200 mV s^{-1} within a potential range from -0.9 to $+0.1$ V (vs. Ag/AgCl). The CV curves of our TPA-Bz and TPA-Py CMPs (Figs. 7a and 7b) had quasi-rectangle-like shapes, confirming that the origin of the capacitance of our materials was electric double layer capacitance (EDLC), similar to that of other carbon substrates. Of note, observed deviation from rectangular shape were attributed to electrode/electrolyte charge mobility boosted due to reactions at electrodes or in the electrolytes or even both. If charges mobilities were reversable, these reactions could be pseudocapacitive as the reversable surface reactions could enhance the charge storage [75−77]. Upon increasing the sweep rate from 5 to 200 mV, the current densities increased while the quasi-rectangular shapes of the CV profiles were maintained, implying good rate ability and rapid kinetics [78, 79].

As displayed in Figs. 7c and 7d, we measured the GCD characteristics of the TPA-Bz and TPA-Py CMPs at current densities between 1 and 20 A g^{-1}. The GCD plots of our CMPs were triangular with a slight bend, confirming the pseudocapacity and EDLC features [80]. Furthermore, the discharging time of the TPA-Py CMP was longer than that of the TPA-Bz CMP, suggesting higher capacitance for the former. We estimated the specific capacitances of the TPA-Bz and TPA-Py CMPs from their corresponding GCD plots, obtaining values of 55.1 and 78 F g^{-1}, respectively, at current density of 1 A g^{-1} (Fig. 8a). The excellent activity of Py-based CMP resulted from the high electrochemical performance of its Py units, its excellent porosity and high conductivity, and the enhanced wettability between the electrode and the electrolyte [81]. As a result, the TPA-Py CMP offered improved hydrophilicity, which increased the accessible space available to electrolyte ions, thereby allowing rapid mass transport and, consequently, improved electrochemical capacitance. We estimated the performance of the TPA-Bz and TPA-Py CMPs supercapacitors from their Ragone plots (Fig. 8b), concluding that the high surface area and high conductivity of the TPA-Py CMP were responsible for its higher energy and power densities. Electrochemical impedance spectroscopy (EIS) confirmed that our CMPs possessed structural stability within the electrical interfaces (Fig. S9). We examined the cyclic stability of our prepared CMPs at a current density 10 A g^{-1}; after 2000 cycles, the capacitance retentions of the TPA-Bz and TPA-Py CMPs were 95.2 and 96.7%, respectively (Figs. 8c and 8d), revealing that both had high cycling stability. Table S5 reveals that the specific capacitances of our synthesized TPA-Bz and TPA-Py CMPs were higher than those of other previously reported porous materials. In comparison, supercapacitors designed with CMPs based on tetrabenzonaphthalene-tetraphenylethylene (TPN-TPE CMP), TBN-carbazole (TBN—Car CMP), and TBN—Car-CMP/SWCNT displayed specific capacitances of 18.45, 18.90, and 53 F g^{-1}, respectively, at 0.5 A g^{-1} [80]; DeBlase et al [82]. reported a specific capacitance of 48 F g^{-1} at 0.1 A g^{-1} for a conjugated organic framework (COF) based on 2,6-diaminoanthraquinone 1,3,5-triformylphloroglucinol (DAAQ−TFP COF);

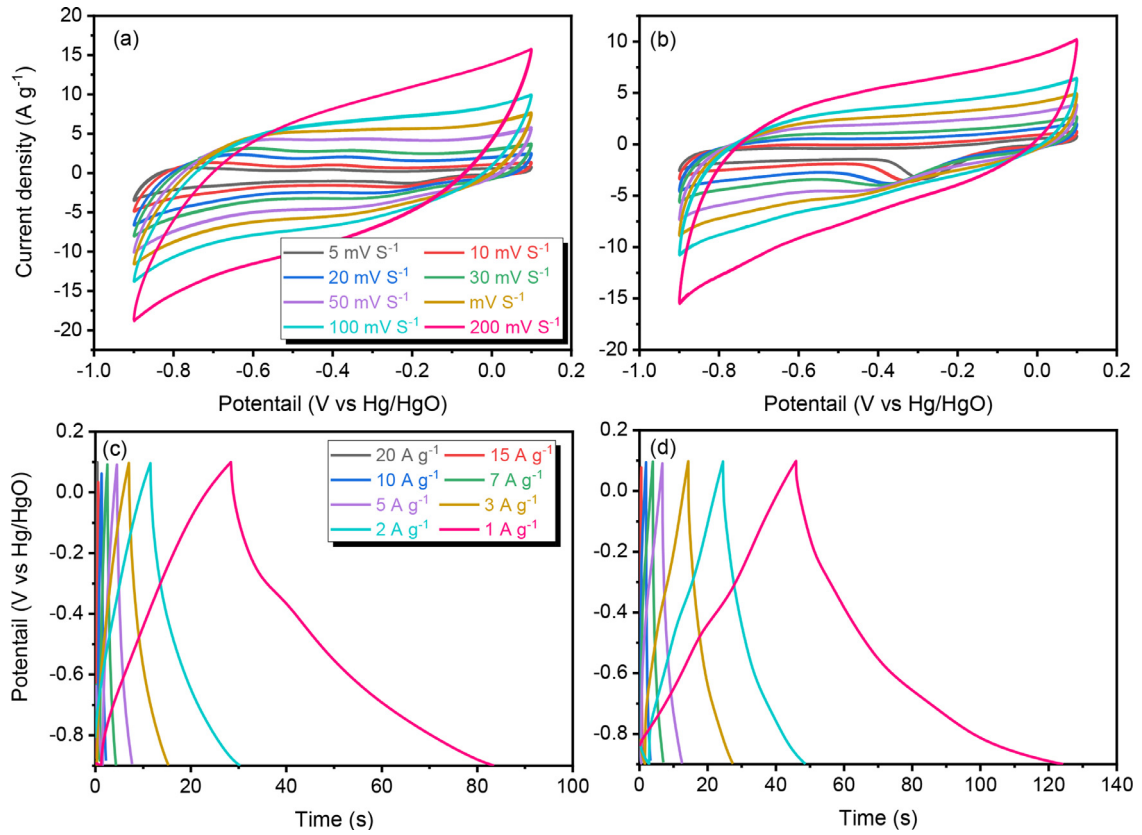**Fig. 7.** (a, b) CV profiles of the (a) TPA-Bz and (b) TPA-Py CMPs. (c, d) GCD spectra of the (c) TPA-Bz and (d) TPA-Py CMPs, measured at various currents.
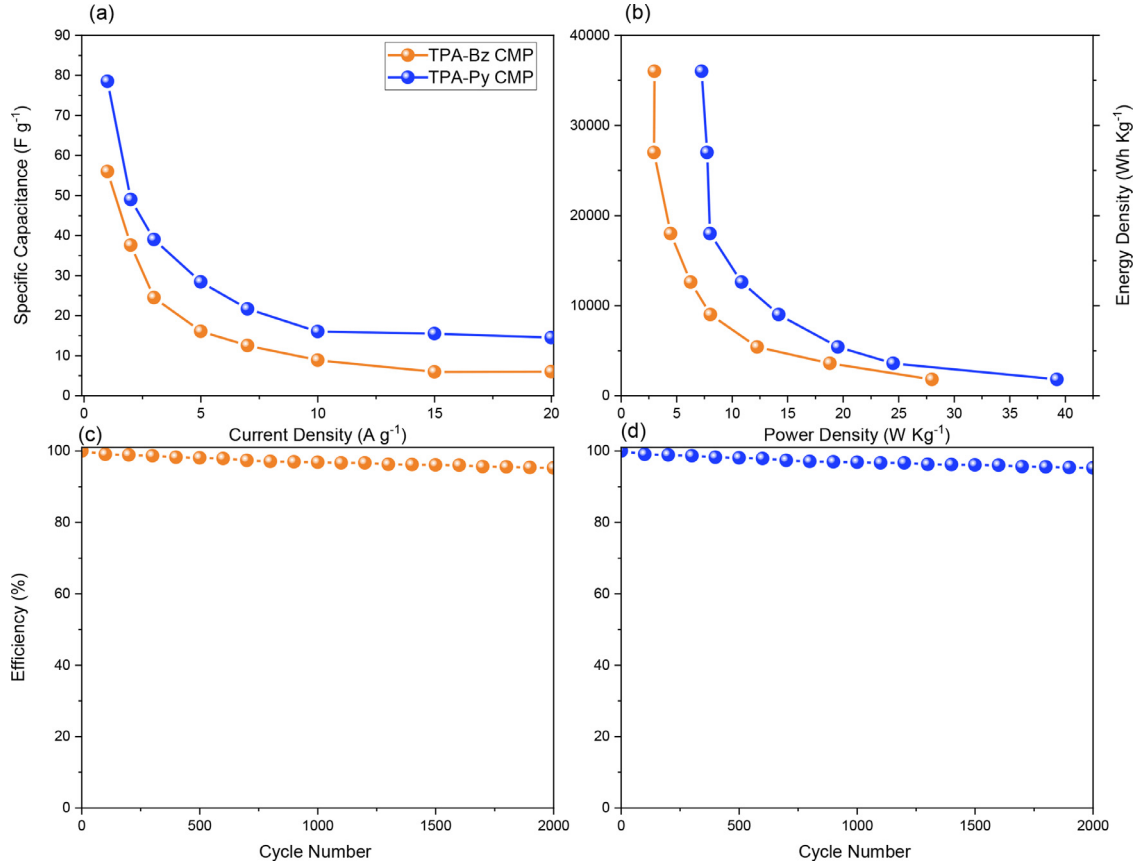

Fig. 8. (a) Specific capacitances of the TPA-Bz and TPA-Py CMPs, measured at current densities from 0.5 to 20 A g^{-1}, (b) Ragone plots of the TPA-Bz and TPA-Py CMPs, cycling stabilities of the (c) TPA-Bz and (d) TPA-Py CMPs, measured at 10 A g^{-1} over 2000 cycles.

El-Mahdy et al [83]. synthesized six COFs based on TPA that displayed specific capacitances of 51.3, 14.4, 5.1, 2.4, 0.34, and 0.24 F g^{-1} at 0.1 A g^{-1}; Park et al [84]. reported specific capacitances of 71 F g^{-1} at 1 A g^{-1} for their N—CMP system and 13.7 F g^{-1} at 1 A g^{-1} for their CoPc-CMP system [85]; and Yang et al [86]. reported an MXene-based conjugated microporous polymer (PAQBz) exhibiting a capacitance of 106 F g^{-1} at 0.3 A g^{-1}.

Conclusion

We have prepared two new TPA-based CMPs that possess outstanding thermal stabilities, high surface areas, and high chemical resistances. We examined these CMPs as adsorbents for purifying water and for energy storage. Our TPA-based CMPs displayed great potential for adsorbing trace pollutants from water. The TPA-Bz and TPA-Py CMPs possessed high adsorption capacities toward the dye RhB in an aqueous environment, with these high adsorption capacities occurring within short periods of time (10 min). Furthermore, these CMPs displayed good efficacy and high stability when used as supercapacitor electrodes. Consequently, TPA-based CMPs appear to be useful as new and efficient materials for both the removal of RhB from wastewater (1633 mg g^{-1}) and for energy storage (78 F g^{-1}). We anticipate that such materials might find applicability in various fields in the near future. Most importantly, we suggest a new strategy-increasing the degrees of conjugation and planarity of monomeric building blocks- for the development of next-generation materials for water treatment and energy storage.

Declaration of Competing Interest

The authors declare that they have no known competing financial interests or personal relationships that could have appeared to influence the work reported in this paper.

Acknowledgments

Supplementary materials

Supplementary material associated with this article can be found, in the online version, at doi:10.1016/j.jtice.2022.104310.

References

[1] Jiang JX, Su F, Trewin A, Wood CD, Campbell NL, Niu H, Dickinson C, Ganin AY, Rosseinsky MJ, Khimyak YZ, Cooper AI. Conjugated microporous poly (arylenee-thynylene) networks. Angew Chem Int Ed 2007;46:8574–8.

[2] Lee J-SM, Cooper AI. Advances in conjugated microporous polymers. Chem Rev 2020;120:2171–214.

[3] Lee T-L, Elewa AM, Kotp MG, Chou H-H, El-Mahdy AFM. Carbazole-and thiophene-containing conjugated microporous polymers with different planarity for enhanced photocatalytic hydrogen evolution. Chem Commun 2021;57:11968–71.

[4] Han S, Li Z, Ma S, Zhi Y, Xia H, Chen X, Liu X. Bandgap engineering in benzotrithiophene-based conjugated microporous polymers: a strategy for screening metal-free heterogeneous photocatalysts. J Mater Chem A 2021;9:3333–40.

[5] Mohamed MG, EL-Mahdy AFM, Kotp MG, Kuo S-W. Advances in porous organic polymers: syntheses, structures, and diverse applications. Mater. Adv. 2022;3:707–33.

[6] Elewa AM, EL-Mahdy AFM, Elsayed MH, Mohamed MG, Kuo S-W, Chou H-H. Sulfur-doped triazine-conjugated microporous polymers for achieving the robust visible-light-driven hydrogen evolution. Chem Eng J 2021;421:129825.

[7] Mohamed MG, Chen T-C, Kuo S-W. Solid-State Chemical Transformations to Enhance Gas Capture in Benzoxazine-Linked Conjugated Microporous Polymers. Macromolecules 2021;12:5866–77.

[8] Mohamed MG, Ahmed MM, Du W-T, Kuo S-W. Meso/Microporous carbons from conjugated hyper-crosslinked polymers based on tetraphenylethene for high-performance CO2 capture and supercapacitor. Molecules 2021;26:738.

[9] Mohamed MG, Atayde Jr EC, Matsagar BM, Na J, Yamauchi Y, Wu KC-W, Kuo S-W. Construction hierarchically mesoporous/microporous materials based on block copolymer and covalent organic framework. J Taiwan Inst Chem Eng 2020;112:180–92.

[10] Konstas K, Taylor JW, Thornton AW, Doherty CM, Lim WX, Bastow TJ, Kennedy DF, Wood CD, Cox BJ, Hill JM. Lithiated porous aromatic frameworks with exceptional gas storage capacity. Angew Chem 2012;124:6743–6.

[11] Babarao R, Dai S, Jiang D-e. Functionalizing porous aromatic frameworks with polar organic groups for high-capacity and selective CO2 separation: a molecular simulation study. Langmuir 2011;27:3451–60.

[12] Xi E, Zhao Y, Xie Y, Gao N, Bian Z, Zhu G. Biological application of porous aromatic frameworks: state of the art and opportunities. J Phys Chem Lett 2021;12:11050–60.

[13] Mohamed MG, Elsayed MH, Elewa AM, EL-Mahdy AFM, Yang C-H, Mohammed AA, Chou H-H, Kuo S-W. Pyrene-containing conjugated organic microporous polymers for photocatalytic hydrogen evolution from water. Catal Sci Technol 2021;11:2229–41.

[14] Qian Z, Wang ZJ, Zhang KA. Covalent Triazine Frameworks as Emerging Heterogeneous Photocatalysts. Chem Mater 2021;33:1909–26.

[15] Kotp MG, Elewa AM, EL-Mahdy AFM, Chou H-H, Kuo S-W. Tunable Pyridyl-Based conjugated microporous polymers for visible light-driven hydrogen evolution. ACS Appl. Energy Mater. 2021;4:13140–51.

[16] Barman S, Singh A, Rahimi FA, Maji TK. Metal-free catalysis: a redox-active donor–acceptor conjugated microporous polymer for selective visible-light-driven CO2 Reduction to CH4. J Am Chem Soc 2021;143:16284–92.

[17] Xu H, Li X, Hao H, Dong X, Sheng W, Lang X. Designing fluorene-based conjugated microporous polymers for blue light-driven photocatalytic selective oxidation of amines with oxygen. Appl Catal B. 2021;285:119796.

[18] Cui I, Zhou J, Li C-c, Deng S, Gao W, Zhang X, Luo X, Wang X, Zhang C-y. Bipolar Aggregation-Induced Electrochemiluminescence of Thiophene-Fused Conjugated Microporous Polymers. ACS Appl Mater Interfaces 2021;13:28782–9.

[19] Laybourn A, Dawson R, Clowes R, Hasell T, Cooper AI, Khimyak YZ, Adams DJ. Network formation mechanisms in conjugated microporous polymers. Polym Chem 2014;5:6325–33.

[20] Bonillo B, Sprick RS, Cooper AI. Tuning photophysical properties in conjugated microporous polymers by comonomer doping strategies. Chem Mater 2016;28:3469–80.

[21] Li A, Lu RF, Wang Y, Wang X, Han KL, Deng WQ. Lithium-doped conjugated microporous polymers for reversible hydrogen storage. Angew Chem 2010;122:3402–5.

[22] Tantisriyanurak S, Duguid HN, Peattie L, Dawson R. Acid functionalized conjugated microporous polymers as a reusable catalyst for biodiesel production. ACS Appl Polym Mater 2020;2:3908–15.

[23] Schmidt J, Weber J, Epping JD, Antonietti M, Thomas A. Microporous conjugated poly (thienylene arylene) networks. Adv Mater 2009;21:702–5.

[24] Zhou Y-B, Wang Y-Q, Ning L-C, Ding Z-C, Wang W-L, Ding C-K, Li R-H, Chen J-J, Lu X, Ding Y-J. Conjugated microporous polymer as heterogeneous ligand for highly selective oxidative Heck reaction. J Am Chem Soc 2017;139:3966–9.

[25] Wu K, Guo J, Wang C. Gelation of metalloporphyrin-based conjugated microporous polymers by oxidative homocoupling of terminal alkynes. Chem Mater 2014;26:6241–50.

[26] Battula VR, Singh H, Kumar S, Bala I, Pal SK, Kailasam K. Natural sunlight driven oxidative homocoupling of amines by a truxene-based conjugated microporous polymer. ACS Catal 2018;8:6751–9.

[27] Chen Q, Han BH. Microporous polycarbazole materials: from preparation and properties to applications. Macromol Rapid Commun 2018;39:1800040.

[28] Li B, Guan Z, Wang W, Yang X, Hu J, Tan B, Li T. Highly dispersed Pd catalyst locked in knitting aryl network polymers for Suzuki–Miyaura coupling reactions of aryl chlorides in aqueous media. Adv Mater 2012;24:3390–5.

[29] Mohamed MG, Liu N-Y, EL-Mahdy AFM, Kuo S-W. Ultrastable luminescent hybrid microporous polymers based on polyhedral oligomeric silsesquioxane for CO2 uptake and metal ion sensing. Microporous Mesoporous Mater 2021;311:110695.

[30] Samy MM, Mohamed MG, Mansoure TH, Meng TS, Khan MAR, Liaw C-C, Kuo S-W. Solid state chemical transformations through ring-opening polymerization of ferrocene-based conjugated microporous polymers in host−guest complexes with benzoxazine-linked cyclodextrin. J Taiwan Inst Chem Eng 2022;132:104110.

[31] Ouyang Z, Tranca D, Zhao Y, Chen Z, Fu X, Zhu J, Zhai G, Ke C, Kymakis E, Zhuang X. Quinone-Enriched Conjugated Microporous Polymer as an Organic Cathode for Li-Ion Batteries. ACS Appl Mater Interfaces 2021;13:9064–73.

[32] EL-Mahdy AFM, Elewa AM, Huang SW, Chou HH, Kuo SW. Dual-function fluorescent covalent organic frameworks: hCl sensing and photocatalytic H2 evolution from water. Adv Opt Mater 2020;8:2000641.

[33] Song Y, Lan PC, Martin K, Ma S. Rational design of bifunctional conjugated microporous polymers. Nanoscale Adv 2021;3:4891–906.

[34] Chen J, Yan W, Townsend EJ, Feng J, Pan L, Del Angel Hernandez V, Faul CF. Tunable surface area, porosity, and function in conjugated microporous polymers. Angew Chem Int Ed 2019;58:11715–9.

[35] Li X, Ma X, Zhang F, Dong X, Lang X. Selective photocatalytic formation of sulfoxides by aerobic oxidation of sulfides over conjugated microporous polymers with thiazolo [5, 4-d] thiazole linkage. Appl Catal B 2021;298:120514.

[36] Ren D, Ren S, Lin Y, Xu J, Wang X. Recent developments of organic solvent resistant materials for membrane separations. Chemosphere 2021;271:129425.

[37] Kotp MG, EL-Mahdy AFM, Yang T-L, Kuo S-W. A pyridinyl-phenanzine conjugated microporous polymer decorated with ultrafine Ag nanoparticles mediates the rapid reduction of nitrophenol. Microporous Mesoporous Mater 2022;331:111669.

[38] Luo S, Zeng Z, Wang H, Xiong W, Song B, Zhou C, et al. Recent Progress in Conjugated Microporous Polymers for Clean Energy: synthesis, Modification, Computer Simulations, and Applications. Prog Polym Sci 2021;115:101374.

[39] Mohamed MG, Lee C-C, EL-Mahdy AFM, Lüder J, Yu M-H, Li Z, Zhu Z, Chueh C-C, Kuo S-W. Exploitation of two-dimensional conjugated covalent organic frameworks based on tetraphenylethylene with bicarbazole and pyrene units and applications in perovskite solar cells. J Mater Chem A 2020;8:11448–59.

[40] Lu H, Shi W, Zhao F, Zhang W, Zhang P, Zhao C, Yu G. High-Yield and Low-Cost Solar Water Purification via Hydrogel-Based Membrane Distillation. Adv Funct Mater 2021;31:2101036.

[41] Zhou W, Zhang W, Cai Y. Laccase immobilization for water purification: a comprehensive review. Chem Eng J 2021;403:126272.

[42] Zhang M, Cui J, Lu T, Tang G, Wu S, Ma W, Huang C. Robust, functionalized reduced graphene-based nanofibrous membrane for contaminated water purification. Chem Eng J 2021;404:126347.

[43] Mohamed MG, Kuo S-W. Crown ether-functionalized polybenzoxazine for metal ion adsorption. Macromolecules 2020;53:2420–9.

[44] Xiao P, He J, Ni F, Zhang C, Liang Y, Zhou W, Gu J, Xia J, Kuo S-W, Chen T. Exploring interface confined water flow and evaporation enables solar-thermal-electro integration towards clean water and electricity harvest via asymmetric functionalization strategy. Nano Energy 2020;68:104385.

[45] Ejeta DD, Wang C-F, Kuo S-W, Chen J-K, Tsai H-C, Hung W-S, Hu C-C, Lai J-Y. Preparation of superhydrophobic and superoleophilic cotton-based material for extremely high flux water-in-oil emulsion separation. Chem Eng J 2020;402:126289.

[46] Zhang C, Xiao P, Ni F, Gu J, Chen J, Nie Y, Kuo S-W, Chen T. Breathable and superhydrophobic photothermic fabric enables efficient interface energy management via confined heating strategy for sustainable seawater evaporation. Chem Eng J 2022;428:131142.

[47] Ayad MM, Amer WA, Kotp MG. Magnetic polyaniline-chitosan nanocomposite decorated with palladium nanoparticles for enhanced catalytic reduction of 4-nitrophenol. Mol Catal 2017;439:72–80.

[48] Ayad MM, Amer WA, Kotp MG, Minisy IM, Rehab AF, Kopecký D, Fitl P. Synthesis of silver-anchored polyaniline−chitosan magnetic nanocomposite: a smart system for catalysis. RSC Adv 2017;7:18553–60.

[49] Tkaczyk A, Mitrowska K, Posyniak A. Synthetic organic dyes as contaminants of the aquatic environment and their implications for ecosystems: a review. Sci Total Environ 2020;717:137222.

[50] Wainwright M. Dyes in the development of drugs and pharmaceuticals. Dyes Pigm 2008;76:582–9.

[51] Lellis B, Fávaro-Polonio CZ, Pamphile JA, Polonio JC. Effects of textile dyes on health and the environment and bioremediation potential of living organisms. Biotechnol Res Innov 2019;3:275–90.

[52] Quan Y, Shi W, Song Y, Jiang X, Wang C, Lin W. Bifunctional metal−organic layer with organic dyes and iron centers for synergistic photoredox catalysis. J Am Chem Soc 2021;143:3075–80.

[53] Gupta K, Khatri OP. Fast and efficient adsorptive removal of organic dyes and active pharmaceutical ingredient by microporous carbon: effect of molecular size and charge. Chem Eng J 2019;378:122218.

[54] El-Mahdy AFM, Liu T-E, Kuo S-W. Direct synthesis of nitrogen-doped mesoporous carbons from triazine-functionalized resol for CO2 uptake and highly efficient removal of dyes. J Hazard Mater 2020;391:122163.

[55] El-Mahdy AFM, Young C, Kim J, You J, Yamauchi Y, Kuo S-W. Hollow microspherical and microtubular [3+ 3] carbazole-based covalent organic frameworks and their gas and energy storage applications. ACS Appl Mater Interfaces 2019;11:9343–54.

[56] Zhao X, Liu S, Tang Z, Niu H, Cai Y, Meng W, Wu F, Giesy JP. Synthesis of magnetic metal-organic framework (MOF) for efficient removal of organic dyes from water. Sci Rep 2015;5:11849.

[57] Abdi J, Vossoughi M, Mahmoodi NM, Alemzadeh I. Synthesis of metal-organic framework hybrid nanocomposites based on GO and CNT with high adsorption capacity for dye removal. Chem Eng J 2017;326:1145–58.

[58] Septiani NLW, Kaneti YV, Fathoni KB, Wang J, Ide Y, Yuliarto B, Dipojono HK, Nanjundan AK, Golberg D, Bando Y. Self-assembly of nickel phosphate-based nanotubes into two-dimensional crumpled sheet-like architectures for high-performance asymmetric supercapacitors. Nano Energy 2020;67:104270.

[59] Tang J, Salunkhe RR, Zhang H, Malgras V, Ahamad T, Alshehri SM, Kobayashi N, Tominaka S, Ide Y, Kim JH. Bimetallic metal-organic frameworks for controlled catalytic graphitization of nanoporous carbons. Sci Rep 2016;6:1–8.

[60] Rafatullah M, Sulaiman O, Hashim R, Ahmad A. Adsorption of methylene blue on low-cost adsorbents: a review. J Hazard Mater 2010;177:70–80.

[61] Wang J, Wang Y, Hu H, Yang Q, Cai J. From metal−organic frameworks to porous carbon materials: recent progress and prospects from energy and environmental perspectives. Nanoscale 2020;12:4238–68.

[62] Xu X, Tang J, Qian H, Hou S, Bando Y, Hossain MSA, Pan L, Yamauchi Y. Three-dimensional networked metal−organic frameworks with conductive polypyrrole tubes for flexible supercapacitors. ACS Appl Mater Interfaces 2017;9:38737–44.

[63] Cias P, Slugovc C, Gescheidt G. Hole transport in triphenylamine based OLED devices: from theoretical modeling to properties prediction. J Phys Chem A 2011;115:14519–25.

[64] Shen P, Tang Y, Jiang S, Chen H, Zheng X, Wang X, Zhao B, Tan S. Efficient triphenylamine-based dyes featuring dual-role carbazole, fluorene and spirobifluorene moieties. Org Electron 2011;12:125–35.

[65] Xiong S, Liu J, Wang Y, Wang X, Chu J, Zhang R, Gong M, Wu B. Solvothermal synthesis of triphenylamine-based covalent organic framework nanofibers with excellent cycle stability for supercapacitor electrodes. J Appl Polym Sci 2022;139:51510.

[66] Topal S, Ipek OS, Sezer E, Ozturk T. Electrochromic-hybrid energy storage material consisting of Triphenylamine and Dithienothiophene. Chem Eng J 2021:133868.

[67] Yurchenko O, Freytag D, zur Borg L, Zentel R, Heinze J r, Ludwigs S. Electrochemically induced reversible and irreversible coupling of triarylamines. J Phys Chem B. 2012;116:30–9.

[68] Gong Y, Zhan X, Li Q, Li Z. Progress of pyrene-based organic semiconductor in organic field effect transistors. Sci China Chem. 2016;59:1623–31.

[69] Wang L, Zhou W, Tang Q, Yang H, Zhou Q, Zhang X. Rhodamine-functionalized mechanochromic and mechanofluorescent hydrogels with enhanced mechanoresponsive sensitivity. Polymers (Basel) 2018; 10:994.

[70] Wu C-H, Tu C-W, Aimi J, Zhang J, Chen T, Wang C-C, Huang C-F. Mechanochromic double network hydrogels as a compression stress sensor. Polym Chem 2020;11:6423–8.

[71] Minisy IM, Salahuddin NA, Ayad MM. Adsorption of methylene blue onto chitosan−montmorillonite/polyaniline nanocomposite. Appl Clay Sci 2021;203:105993.

[72] Freundlich H. Over the adsorption in solution. J. Phys. chem 1906;57:1100–7.

[73] Langmuir I. The adsorption of gases on plane surfaces of glass, mica and platinum. J Am Chem Soc 1918;40:1361–403.

[74] Saber AF, Chen K-Y, EL-Mahdy AFM, Kuo S-W. Designed azo-linked conjugated microporous polymers for CO2 uptake and removal applications. J Polym Res 2021;28:430.

[75] EL-Mahdy AFM, Zakaria MB, Wang H-X, Chen T, Yamauchi Y, Kuo S-W. Heteroporous bifluorenylidene-based covalent organic frameworks displaying exceptional dye adsorption behavior and high energy storage. J Mater Chem A 2020;8:25148–55.

[76] Mohamed MG, EL-Mahdy AFM, Ahmed MM, Kuo SW. Direct synthesis of microporous bicarbazole-based covalent triazine frameworks for high-performance energy storage and carbon dioxide uptake. Chempluschem 2019; 84:1767–74.

[77] EL-Mahdy AFM, Yu TC, Kuo S-W. Synthesis of multiple heteroatom−doped mesoporous carbon/silica composites for supercapacitors. Chem Eng J 2021;414:128796.

[78] Khattak AM, Ghazi ZA, Liang B, Khan NA, Iqbal A, Li L, Tang Z. A redox-active 2D covalent organic framework with pyridine moieties capable of faradaic energy storage. J Mater Chem A 2016;4:16312–7.

[79] El-Mahdy AFM, Lüder J, Kotp MG, Kuo S-W. A Tröger's base-derived covalent organic polymer containing carbazole units as a high-performance supercapacitor. Polymers (Basel) 2021; 13:1385.

[80] Samy MM, Mohamed MG, El-Mahdy AFM, Mansoure TH, Wu KC-W, Kuo S-W. High-performance supercapacitor electrodes prepared from dispersions of Tetrabenzonaphthalene-based conjugated microporous polymers and carbon nanotubes. ACS Appl Mater Interfaces 2021;44:51906–16.

[81] Li Z, Zhang W, Wang H, Qin Z. Activated pyrene decorated graphene with enhanced performance for electrochemical energy storage. Chem Eng J 2018;334:845–54.

[82] DeBlase CR, Silberstein KE, Truong T-T, Abruña HD, Dichtel WR. β-Ketoenamine-linked covalent organic frameworks capable of pseudocapacitive energy storage. J Am Chem Soc 2013;135:16821–4.

[83] El-Mahdy AFM, Kuo C-H, Alshehri A, Young C, Yamauchi Y, Kim J, Kuo S-W. Strategic design of triphenylamine-and triphenyltriazine-based two-dimensional covalent organic frameworks for CO 2 uptake and energy storage. J Mater Chem A 2018;6:19532–41.

[84] Park SY, Kang CW, Lee SM, Kim HJ, Ko Y-J, Choi J, Son SU. Nanoparticulate conjugated microporous polymer with post-modified Benzils for enhanced Pseudocapacitor performance. Chem. Eur. J 2020;26:12343–8.

[85] Mei L, Cui X, Duan Q, Li Y, Lv X, Wang H-g. Metal phthalocyanine-linked conjugated microporous polymer hybridized with carbon nanotubes as a high-performance flexible electrode for supercapacitors. Int J Hydrog Energy 2020;45:22950–8.

[86] Yang W, Huang B, Li L, Zhang K, Li Y, Huang J, Tang X, Hu T, Yuan K, Chen Y. Covalently sandwiching MXene by conjugated microporous polymers with excellent stability for supercapacitors. Small Methods 2020;4:2000434.